Magnetic Snell's law and spin-wave fiber with Dzyaloshinskii-Moriya interaction

Weichao Yu (□□□), Jin Lan (□□), Ruqian Wu, and Jiang Xiao (□□)

Phys. Rev. B **94**, 140410 — Published 11 October 2016

DOI: 10.1103/PhysRevB.94.140410

A magnonic Snell's law and spin wave fiber with Dzyaloshinskii-Moriya interaction

Weichao Yu (余伟超),[1,*] Jin Lan (兰金),[1,*] Ruqian Wu,[1,2] and Jiang Xiao (萧江)[1,3,†]

[1]*Department of Physics and State Key Laboratory of Surface Physics, Fudan University, Shanghai 200433, China*
[2]*Department of Physics and Astronomy, University of California, Irvine, California 92697-4575, USA*
[3]*Collaborative Innovation Center of Advanced Microstructures, Fudan University, Shanghai 200433, China*

Spin waves are collective excitations propagating in the magnetic medium with ordered magnetizations. Magnonics, utilizing the spin wave (magnon) as information carrier, is a promising candidate for low-dissipation computation and communication technologies. We discover that, due to the Dzyaloshinskii-Moriya interaction, the scattering behavior of spin wave at a magnetic domain wall follows a generalized Snell's law, where two magnetic domains work as two different mediums. Similar to optical total reflection that occurs at the water-air interfaces, spin waves may experience total reflection at magnetic domain walls when their incident angle larger than a critical value. We design a spin wave fiber using a magnetic domain structure with two domain walls, and demonstrate that such a spin wave fiber can transmit spin waves over long distance by total internal reflections, in analogy to an optical fiber. Our design of spin wave fiber opens up new possibilities in pure magnetic information processing.

A trend in post-silicon information processing is to develop systems that employ (quasi-) particles other than electrons as the information carriers to avoid the Joule heating. One of the most promising candidates is magnonics [1, 2], which transfers information through collective excitations of magnetization, or called spin waves (magnons). The crucial advantage of spin waves is that they can propagate in both conducting and insulating magnetic materials without physical motion of electrons. This enables the development of insulator-based systems that produce no Joule heating at all. In addition, spin waves can be manipulated via magnetic structures in a single material rather than the heterogenous structures consisting of different materials. This makes it possible to realize a rewritable spin wave logic architecture [3]. Due to these desirable features, magnonics becomes a new realm of active interdisciplinary research and has witnessed rapid and fruitful developments in recent years. [3–8].

The World Wide Web, one of the most important infrastructures of the modern society, would not be possible without the optical fiber, which can transmit information over long distance. An optical fiber is made of two dielectric materials with different indices of refraction [9]. The defining feature of an optical fiber is the total reflection at the interface between the two dielectric materials. Here we report a design of the spin wave fiber that can transmit spin waves in magnonic chips using the total reflection at magnetic domain walls, in an analog of the optical fiber. The design is based on a magnetic domain structure with two domain walls, at which spin waves are totally reflected due to the Dzyaloshinskii-Moriya interaction (DMI) [10, 11], an asymmetric magnetic interaction induced by the spin-orbit interaction. Instead of two dielectric materials used in an optical fiber, it is feasible and convenient to use one single material but different magnetic domains in a spin wave fiber. Typically, the spin wave dispersion relation does not vary much across magnetic domains. However, the DMI leads to domain-dependent dispersions, which gives rise to a total reflection of spin waves at the domain walls.

Model. We consider a magnetic thin film with two magnetic domains, whose magnetizations point in opposite directions with a Bloch domain wall in between as shown in Fig. 1. The film is in the x-y plane and the magnetization in the left/right domain is along $\mp\hat{\mathbf{y}}$ direction, respectively. The domain wall is also along $\hat{\mathbf{y}}$ direction. The magnetic dynamics is described by the Landau-Lifshitz-Gilbert (LLG) equation,

$$\frac{\partial \mathbf{m}}{\partial t} = -\gamma \mathbf{m} \times \mathbf{H}_{\text{eff}} + \alpha_{\text{G}} \mathbf{m} \times \frac{\partial \mathbf{m}}{\partial t}, \tag{1}$$

where $\mathbf{m}(\mathbf{r}, t)$ is the unit vector representing the magnetization direction, γ is the gyromagnetic ratio, α_{G} is the Gilbert damping parameter, and $\gamma \mathbf{H}_{\text{eff}} = K m_y \hat{\mathbf{y}} + A\nabla^2 \mathbf{m} - D\nabla \times \mathbf{m}$ is the effective magnetic field with K the magnetic uniaxial anisotropy (along $\hat{\mathbf{y}}$ direction), A the exchange coupling constant, and D the parameter for the DMI. Let $\mathbf{m}_0$ be the static magnetization direction, and $\delta\mathbf{m}(\mathbf{r}, t) = m_\theta \hat{\mathbf{e}}_\theta + m_\phi \hat{\mathbf{e}}_\phi$ be the dynamical excitation on top of the static $\mathbf{m}_0(\mathbf{r})$, with $\hat{\mathbf{e}}_{\theta,\phi} \perp \mathbf{m}_0$ as the two transverse directions to $\mathbf{m}_0$. In the small excitation approximation ($m_{\theta,\phi} \ll 1$), the spin wave dispersion relations in the left/right domain with $\mathbf{m}_0 = \mp\hat{\mathbf{y}}$ are [12, 13]

$$\omega(\mathbf{k}) = K + A(k_x^2 + k_y^2) \mp D k_y, \tag{2}$$

where $\mathbf{k} = (k_x, k_y)$ is the spin wave wavevector. In the absence of DMI ($D = 0$), the spin waves with frequency ω form a circle centered at the origin in the $\mathbf{k}$-space. However, the DMI, in the last term in Eq. (2), pushes the isofrequency circle by $\Delta = D/2A$ in the direction of $-\mathbf{m}_0$ as depicted separately for the two domains in Fig. 1. The spin wave group velocity is $\mathbf{v}_g = \partial\omega/\partial\mathbf{k} = 2A(\mathbf{k} \mp \hat{\mathbf{y}}\Delta) \equiv 2A\mathbf{k}_g^{\mp}$, where $\left|\mathbf{k}_g^{\mp}\right| = k_g(\omega) = \sqrt{(\omega - K)/A + \Delta^2}$ is the radius of the isofrequency circle. Other methods of modifying the dispersion include the magnonic crystals employing magnetic superlattices [1, 14], and the gradient-index magnonics employing non-uniform effective magnetic field configurations [15, 16].

Magnonic Snell's law. An important consequence of the opposite shifts of the isofrequency circles in the left and right domains is spin wave refraction across the domain wall. When the spin wave strikes from left domain with an incident angle

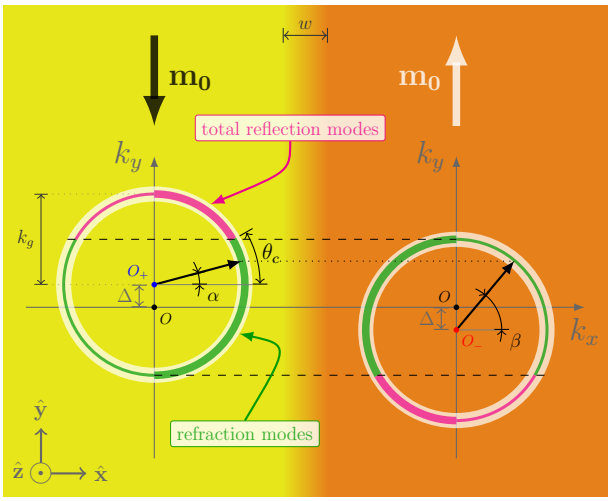

Figure 1. Schematic of the magnonic Snell's law. A domain wall structure with magnetization pointing in $\mathbf{m}_0(\mathbf{r}) = \mp\hat{\mathbf{y}}$ in the left/right domain and $\mathbf{m}_0$ continuously rotates from $-\hat{\mathbf{y}}$ to $+\hat{\mathbf{y}}$ over a domain wall width w as depicted in the upper right inset. The isofrequency circles in the wavevector space are shifted for two magnetic domains with opposite magnetizations when DMI is present. The spin wave modes on both circles have the same frequency ω. The modes on the thick green segment can be refracted into the other domain because there exist propagating modes with the same k_y on the isofrequency circle across the domain wall. However, the modes on the thick magenta segment cannot pass and must be totally reflected due to the lack of the propagating modes with the same k_y across the domain wall.

α (angle of the group velocity with respect to the domain wall normal $+\hat{\mathbf{x}}$ direction), it is refracted to a mode with an outgoing angle β in the right domain. To guarantee continuity of the wavevector (k_y) along the domain wall, the refraction angle obeys the generalized Snell's law,

$$k_g \sin\alpha + \Delta = k_g \sin\beta - \Delta. \tag{3}$$

This is an analogy of the generalized Snell's law in photonics [17–21] and phononics [22, 23] across meta-surfaces, in which a phase gradient is introduced at the interface between two mediums by sub-wavelength engineering. In comparison to the complicated meta-surfaces in its optical and acoustic counterparts, it is much easier and more straightforward to realize the non-trivial Snell's law in magnonics, *i.e.*, simply by introducing DMI in the whole film with no sub-wavelength structures. The Snell's law in Eq. (3) is derived for an interface (domain wall) formed by two opposite magnetic domains in a single magnetic material, thus it is completely different from the Snell's laws that were derived for an interface between two regions with different magnetic properties [24, 25]. In addition, Eq. (3) also share some similarity with the Snell's law studied in graphene [26], in which the refraction and reflection occur at an interface between two regions subjecting to different strains. The generalized magnonic Snell's law can lead to the anomalous negative refraction [24, 27, 28]. Note that in Fig. 1 the static magnetization in the left/right domain $\mathbf{m}_0 = \mp\hat{\mathbf{y}}$ is parallel to the domain wall. In a general situation where $\mathbf{m}_0$ in the left/right domain forms an angle $\pm\xi$ with the domain wall (along $\hat{\mathbf{y}}$), the offset of the isofrequency circle along $\hat{\mathbf{y}}$ is reduced to $\Delta\cos\xi$, thus Eq. (3) is modified with a substitution $\Delta \to \Delta\cos\xi$. When demagnetization field is included, the magnonic Snell's law in Eq. (3) remains basically the same (See Supplementary Materials).

According to the magnonic Snell's law in Eq. (3), total reflection occurs when the incident angle α satisfies $\theta_c < \alpha < \pi/2$ (the thick magenta segment in Fig. 1) with the critical angle (provided $k_g(\omega) > \Delta$)

$$\theta_c = \arcsin\left[1 - \frac{2\Delta}{k_g(\omega)}\right]. \tag{4}$$

As a result, the modes with incident angle $-\pi/2 < \alpha < \theta_c$ (the thick green segment in Fig. 1) are refracted into the right domain. Depending on value of $\Delta/k_g(\omega)$ (thus on D and ω), the critical angle θ_c can take any value between $-\pi/2$ and $\pi/2$. For instance, when there is no DMI ($D = 0$), $\theta_c = \pi/2$ and all incident modes are transmitted and no total reflection occurs. When D is strong (or ω is small) such that the offset between the two isofrequency circles $\Delta > k_g(\omega)$, $\theta_c = -\pi/2$ and all incident modes are totally reflected.

Semiclassical picture. The magnetic texture of a domain wall can be described by $\mathbf{m}_0(x) = (\sin\theta_0\cos\phi_0, \sin\theta_0\sin\phi_0, \cos\theta_0)$, where $\theta_0(x), \phi_0(x)$ are the polar and azimuthal angle of $\mathbf{m}_0$ with respect to $\hat{\mathbf{z}}$. For a Bloch type domain wall, in the presence of DMI ($D \neq 0$), a Walker configuration with $\phi_0(x) = \pi/2$, $\theta_0(x) = -\pi/2 - 2\mathrm{sign}(D)\arctan[\exp(x/w)]$ is stable, where $w = \sqrt{A/K}$ is the domain wall width. By rewriting the dynamical excitation $\delta\mathbf{m}$ as $\psi = m_\theta - im_\phi$, Eq. (1) can be recast to a Schrödinger-like equation [3, 29, 30]:

$$i\hbar\frac{\partial\psi}{\partial t} = \left[\frac{1}{2m^*}\left(\hat{\mathbf{p}} - \frac{e}{c}\mathbf{A}\right)^2 + V\right]\psi, \tag{5}$$

where e is the electric charge, $m^* = \hbar/2A$ is the effective mass, $\hat{\mathbf{p}} = -i\hbar\nabla$ is the momentum operator, $V(x) = K[1 - 2\mathrm{sech}^2(x/w)]$ is the texture-induced effective scalar potential, and $\mathbf{A}(x) = -(Dm^*e/c)\tanh(x/w)\hat{\mathbf{y}}$ is the DMI-induced effective vector potential, which gives rise to an effective magnetic field $\mathbf{B}(x) = \nabla\times\mathbf{A} = -(Dm^*e/cw)\mathrm{sech}^2(x/w)\hat{\mathbf{z}}$. As $x/w \to \pm\infty$, the vector potential $\mathbf{A}(x) \to \pm D/2A$, which corresponds to the shift of k_y mentioned above in the left/right domain as in Eq. (2). With Eq. (5), the scattering behavior for spin waves by a domain wall is the same as that for an electron by a scalar potential V and a vector potential $\mathbf{A}$.

This scalar potential $V(x)$ is special because of its reflectionless [29], thus the spin wave scattering behavior is mostly dominated by the vector potential and the associated magnetic field. The field $\mathbf{B}(x)\|\hat{\mathbf{z}}$ is perpendicular to the film, and only exists in the domain wall region, as denoted by the symbol $\odot$ in Fig. 2(a). According to Eq. (3), the incident and the refracted angles satisfy $-\pi/2 \leq \alpha < \beta \leq \pi/2$ (for $D > 0$), thus the spin wave trajectory should always bend

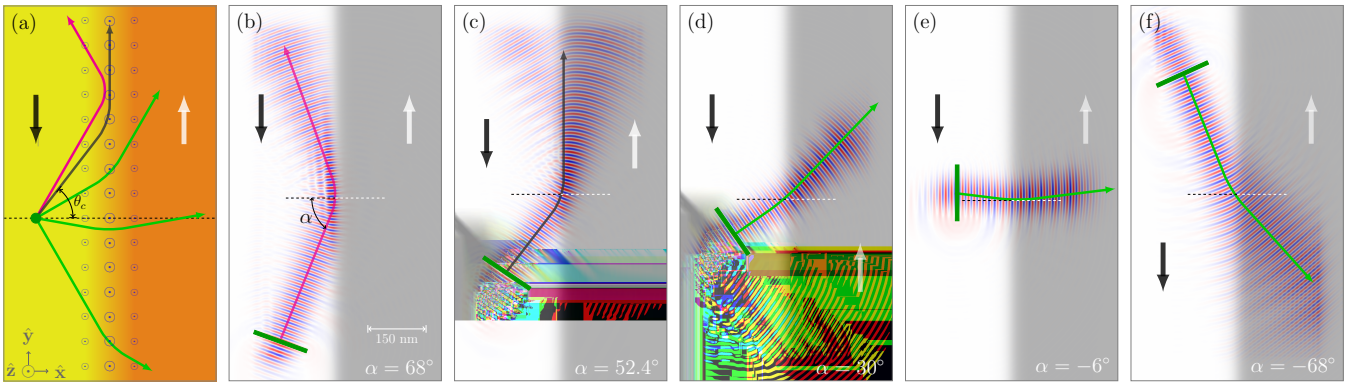

Figure 2. Schematic diagram (a) and the magnetic simulations (b-f) for spin wave reflection and refraction at a magnetic domain wall. The black/white arrow denotes the magnetization direction in the left/right domain colored by yellow/orange (white/gray) in the schematic diagram (simulations). (a) Schematic diagram of reflection/refraction behavior for spin wave incident from left domain with various incident angles. Magenta: $\alpha > \theta_c$, total reflection; black: $\alpha = \theta_c$, critical case ; green: $\alpha < \theta_c$, refraction. All trajectories are bent counter-clockwise by the effective magnetic field perpendicular to plane (denoted by the symbol $\odot$). (b-f) Magnetic simulations with the incident angle $\alpha = 68^\circ$ (b), $\alpha = \theta_c$ (c), $\alpha = 30^\circ$ (d), $\alpha = -6^\circ$ (e), $\alpha = -68^\circ$ (f). In all panels: the domain wall width $w \sim 30$nm; the green bar denotes the exciting location of the spin wave; the exciting fields frequency is $f = 100$Ghz, and the critical angle is estimated to be $\theta_c = 52.4^\circ$.

counter-clockwise. Fig. 2(a) shows the schematic diagram of the spin wave trajectories for various incident angles: when $\alpha > \theta_c$, the spin wave is totally reflected (magenta trajectory); when $\alpha < \theta_c$, the spin wave is refracted (green trajectories); the black trajectory corresponds to the critical situation with $\alpha = \theta_c$. Such scattering behaviors can all be understood by considering the effective Lorentz force due to the effective magnetic field. Evidently, spin waves striking into such an effective magnetic field region will be bent counter-clockwise due to the effective Lorentz force. Consequently, the spin wave that passes through the magnetic field region (the domain wall region), is refracted in counter-clockwise direction as seen in Fig. 2(a). Moreover, if the incident angle is too shallow ($\alpha > \theta_c$), the Lorentz force is able to bend the trajectory so much that the spin wave is completely turned back, and a total reflection occurs.

Total reflection for micromagnetic simulations. The scattering behaviors discussed above are confirmed by micromagnetic simulations. Fig. 2(b-f) show the micromagnetic simulation for the five different incident angles: $\alpha = 60^\circ, 52.4^\circ, 30^\circ, -6^\circ, -60^\circ$, corresponding to the total reflection (b), critical incidence (c), and refraction (d,e,f). Because of the reflectionlessness of the scalar potential $V(x)$ for a Bloch domain wall, the spin wave refractions as in Fig. 2(d-f) is not accompanied by any reflection, which is different from its optical analog. More interestingly, Fig. 2(e) shows the anomalous negative refraction, *i.e.*, both incident and refracted trajectories lie in the same side of normal direction of the scattering plane (the domain wall). All spin wave beams in Fig. 2(b-f) are bent counter clockwise, as predicted by the magnonic Snell's law Eq. (3) and understood from the semi-classical picture above.

Spin wave fiber. Utilizing the total reflection at the magnetic domain wall, we propose a spin wave fiber design as illustrated in Fig. 3(a). The fiber is consisted of one core magnetic domain sandwiched by two cladding domains with the opposite magnetization direction. Because the effective magnetic fields (directions indicated by the $\otimes$ and $\odot$ symbols in Fig. 3(a)) in the upper and lower domain wall are opposite, the spin wave experiences opposite effective Lorentz forces at the upper and lower domain walls. Consequently, spin waves can be transported in the core domain from left to right by total reflections at both domain walls as indicated by the (magenta) right-going trajectory. In contrast, the spin wave propagating from right to left is refracted (leaked) into the cladding layers. Therefore, this spin wave fiber is unidirectional. However, if the spin wave frequency is small enough such that $\Delta > k_g(\omega)$, the critical angle reaches $\theta_c = -\pi/2$, then total reflections occurs for all spin wave modes in all directions, and the spin wave fiber becomes bidirectional. A simple estimate of the spin wave coherence length [4, 8] is $l_\phi \sim 1/\alpha_G k > 100\ \mu$m, much larger than the typical length of our spin wave fiber structure ($w = \sqrt{A/K} \approx 30$nm), ensuring that the functionality of the spin wave fiber is safe from the damping effect. Apparently, one won't expect to use spin wave fibers to transmit information over long distances as optical fibers. Instead, the spin wave fibers can be used to connect different units within a magnonic chip. Note that the spin wave fiber, making use of the total internal reflection at domain walls, is different from all previous waveguides based on geometric constrictions or material confinements [7, 31].

The transporting feature of the spin wave fiber is confirmed by magnetic simulations. Fig. 3(b) shows the propagation of a spin wave beam excited at the core domain with an incident angle $\alpha > \theta_c$. As expected, the right-going spin wave is totally reflected back to the central core domain without leaking to the cladding domains. In contrast, the left-going spin wave passes the domain wall directly and is leaked into the upper cladding domain as expected. Fig. 3(c) shows the spin wave pattern in a spin wave fiber from the point source located at

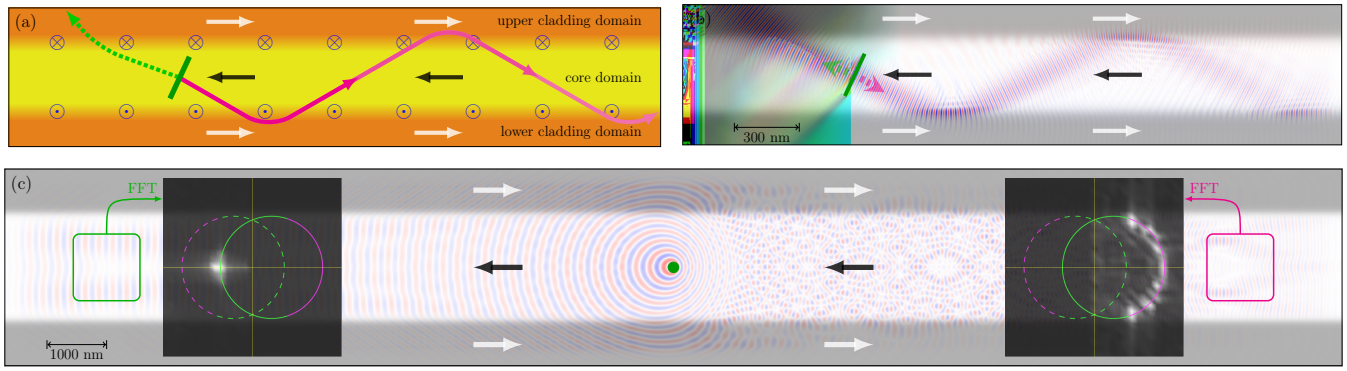

Figure 3. The schematic and the magnetic simulations of a spin wave fiber. The black/white arrow denotes the magnetization direction in the each domain colored by yellow/orange (white/gray) for schematic diagram (simulation). (a) The schematic of the spin wave fiber. The magnetization direction in the central core domain is opposite to that in the upper/lower cladding domain. The solid/dashed trajectory is expected for right/left moving spin waves excited at the green bar. The effective magnetic fields in the upper/lower domain walls point in the opposite directions. Consequently, the right moving spin waves are confined in the central core domain, while the left moving modes are refracted into the cladding domains. (b) The simulated propagation of the spin wave beams excited at green bar with exciting frequency $f = 100$ GHz (critical angle $\theta_c = 52.4°$) and incident angle $\alpha = 62.5°$, confirming the expected paths in (a). (c) The simulated propagation of the spin wave excited by a point source with exciting frequency $f = 10$ GHz. Left/right inset: The Fast Fourier Transformation (FFT) of the spin wave pattern in the region enclosed by the green/magenta box in the far left/right zone. The solid (dashed) circle is for the isofreqency circle of the central (upper/lower) domain, from Eq. (2).

the core domain. The interference pattern of the spin wave on the right side indicates intense reflection of spin wave by the domain walls when propagating rightward, while the simple pattern on the left side indicates the absence of reflection when propagating leftward. By Fourier transforming the spin wave pattern in the highlighted magenta box into $\mathbf{k}$-space, we see that the spin wave modes in the far right falls onto the magenta arc of the isofrequency circle, which corresponds to the total reflection arc in Fig. 1. In contrast, the Fourier transformation of the spin wave in the green box in the far left shows only the direct left moving modes, and all other modes are leaked into the cladding layers by refractions. The exact agreement with the analytical model identifies the critical role of the total reflection in the unidirectionality of the spin wave fiber. In addition, we studied the propagation behaviors of typical eigenmodes in the spin wave fiber, which again highlight the unidirectional transportation features of the spin wave fiber (see Supplementary Materials).

Conclusion. In conclusion, we discovered the generalized magnonic Snell's law that governs the spin wave scattering behavior at a magnetic domain wall in the presence of the Dzyaloshinskii-Moriya interaction. Similar to the optical case, spin waves experience total reflection when the incident angle is larger than a critical angle at a domain wall. Using this property, we designed a spin wave fiber, whose functionality is confirmed by micromagnetic simulations. The proposed spin wave fiber may be used to interconnect different magnonic computation units.

Methods. The simulations are performed in COMSOL Multiphysics using the mathematical module where the LLG equation is transformed into weak form and solved by the generalized-alpha method (amplification of high frequency is 0.6). The sample is a YIG thin film with the following parameters: the easy-axis anisotropy $K/\gamma = 3.88 \times 10^4$ A/m, the exchange constant $A/\gamma = 3.28 \times 10^{-11}$ A $\cdot$ m, the saturation magnetization $M_s = 1.94 \times 10^5$ A/m, the gyromagnetic ratio $\gamma = 2.21 \times 10^5$ rad $\cdot$ Hz/(A/m)[29], and the DMI constant $D/\gamma = 2 \times 10^{-3}$ A [32, 33]. The dipolar interaction is neglected for this operating frequency of exchange spin waves. The Gaussian spin wave beam is prepared by applying an oscillating magnetic field in a narrow rectangle excitation region, where the amplitude of the oscillating field has a Gaussian profile in the transverse direction [34].

Acknowledgements. This work was supported by the National Natural Science Foundation of China under Grant No. 11474065, National Basic Research Program of China under Grant No. 2014CB921600 and No. 2015CB921400. R. W. was also supported by the Department of Energy (U. S.) under Grant No. DE-FG02-05ER46237.

* These authors contributed equally.
† Corresponding author: xiaojiang@fudan.edu.cn

[1] V. V. Kruglyak, S. O. Demokritov, and D. Grundler, J. Phys. D: Appl. Phys. **43**, 264001 (2010).
[2] A. V. Chumak, V. I. Vasyuchka, A. A. Serga, and B. Hillebrands, Nat. Phys. **11**, 453 (2015).
[3] J. Lan, W. Yu, R. Wu, and J. Xiao, Phys. Rev. X **5**, 041049 (2015).
[4] Y. Kajiwara, K. Harii, S. Takahashi, J. Ohe, K. Uchida, M. Mizuguchi, H. Umezawa, H. Kawai, K. Ando, K. Takanashi, S. Maekawa, and E. Saitoh, Nature **464**, 262 (2010).
[5] K. Vogt, F. Fradin, J. Pearson, T. Sebastian, S. Bader, B. Hillebrands, A. Hoffmann, and H. Schultheiss, Nat. Commun. **5**, 3727 (2014).
[6] A. V. Chumak, A. A. Serga, and B. Hillebrands, Nat. Commun.

5, 4700 (2014).
[7] F. Garcia-Sanchez, P. Borys, R. Soucaille, J.-P. Adam, R. L. Stamps, and J.-V. Kim, Phys. Rev. Lett. **114**, 247206 (2015).
[8] R. Cheng, M. W. Daniels, J.-G. Zhu, and D. Xiao, arXiv:1509.05295 [cond-mat] (2015).
[9] J. M. Senior and M. Y. Jamro, *Optical fiber communications: principles and practice* (Pearson Education, 2009).
[10] I. Dzyaloshinsky, J. Phys. Chem. Solids **4**, 241 (1958).
[11] T. Moriya, Phys. Rev. **120**, 91 (1960).
[12] J.-H. Moon, S.-M. Seo, K.-J. Lee, K.-W. Kim, J. Ryu, H.-W. Lee, R. D. McMichael, and M. D. Stiles, Phys. Rev. B **88**, 184404 (2013).
[13] F. Garcia-Sanchez, P. Borys, A. Vansteenkiste, J.-V. Kim, and R. L. Stamps, Phys. Rev. B **89**, 224408 (2014).
[14] R. Gieniusz, V. D. Bessonov, U. Guzowska, A. I. Stognii, and A. Maziewski, Appl. Phys. Lett. **104**, 082412 (2014).
[15] C. S. Davies and V. V. Kruglyak, Low Temp. Phys. **41**, 760 (2015).
[16] G. Duerr, K. Thurner, J. Topp, R. Huber, and D. Grundler, Phys. Rev. Lett. **108**, 227202 (2012).
[17] N. Yu, P. Genevet, M. A. Kats, F. Aieta, J.-P. Tetienne, F. Capasso, and Z. Gaburro, Science **334**, 333 (2011).
[18] N. Yu and F. Capasso, Nat. Mater. **13**, 139 (2014).
[19] S. Sun, Q. He, S. Xiao, Q. Xu, X. Li, and L. Zhou, Nat. Mater. **11**, 426 (2012).
[20] S. Sun, K.-Y. Yang, C.-M. Wang, T.-K. Juan, W. T. Chen, C. Y. Liao, Q. He, S. Xiao, W.-T. Kung, G.-Y. Guo, L. Zhou, and D. P. Tsai, Nano Lett. **12**, 6223 (2012).
[21] X. Chen, L. Huang, H. Mühlenbernd, G. Li, B. Bai, Q. Tan, G. Jin, C.-W. Qiu, S. Zhang, and T. Zentgraf, Nat. Commun. **3**, 1198 (2012).
[22] Y. Li, X. Jiang, R.-q. Li, B. Liang, X.-y. Zou, L.-l. Yin, and J.-c. Cheng, Phys. Rev. Appl. **2**, 064002 (2014).
[23] Y.-F. Zhu, X.-Y. Zou, B. Liang, and J.-C. Cheng, Appl. Phys. Lett. **107**, 113501 (2015).
[24] S.-K. Kim, S. Choi, K.-S. Lee, D.-S. Han, D.-E. Jung, and Y.-S. Choi, Appl. Phys. Lett. **92**, 212501 (2008).
[25] H. Xi, X. Wang, Y. Zheng, and P. J. Ryan, J. Appl. Phys. **104**, 063921 (2008).
[26] Z. Wu, F. Zhai, F. M. Peeters, H. Q. Xu, and K. Chang, Phys. Rev. Lett. **106**, 176802 (2011).
[27] A. V. Vashkovskii and E. H. Lokk, Phys. Usp. **47**, 601 (2004).
[28] E. H. Lock, Phys. Usp. **51**, 375 (2008).
[29] P. Yan, X. S. Wang, and X. R. Wang, Phys. Rev. Lett. **107**, 177207 (2011).
[30] W. Wang, M. Albert, M. Beg, M.-A. Bisotti, D. Chernyshenko, D. Cortes-Ortuno, I. Hawke, and H. Fangohr, Phys. Rev. Lett. **114**, 087203 (2015).
[31] X. Xing and Y. Zhou, NPG Asia Materials **8**, e246 (2016).
[32] T. Liu and G. Vignale, Physical Review Letters **106**, 247203 (2011).
[33] X. Zhang, T. Liu, M. E. Flattè, and H. X. Tang, Physical Review Letters **113**, 037202 (2014).
[34] P. Gruszecki, Y. S. Dadoenkova, N. N. Dadoenkova, I. L. Lyubchanskii, J. Romero-Vivas, K. Y. Guslienko, and M. Krawczyk, Phys. Rev. B **92**, 054427 (2015).